Active-oxygen species on non-reducible rare-earth-oxide-based catalysts in oxidative coupling of methane *

H.B. Zhang, G.D. Lin, H.L. Wan, Y.D. Liu, W.Z. Weng, J.X. Cai, Y.F. Shen and K.R. Tsai **

Department of Chemistry and Institute of Physical Chemistry, Xiamen University, and State Key Laboratory for Physical Chemistry of the Solid Surface, Xiamen 361005, Fujian, PR China
E-mail: krtsai@xmu.edu.cn

Received 14 November 2000; accepted 16 March 2001

From supplementary *in situ* Raman spectroscopic studies of active-oxygen species on non-reducible rare-earth-oxide-based catalysts in the oxidative coupling of methane (OCM) and structural adaptability considerations, further support has been obtained for our proposal that there may be an active and elusive precursor (of $\underline{O}_2^-$ and $\underline{O}_2^{2-}$ adspecies), most probably $\underline{O}_3^{2-}$ formed from reversible redox coupling of an $\underline{O}_2$ adspecies at an anionic vacancy with a neighboring O^{2-} in the surface lattice. This active precursor may initiate H abstraction from CH_4 and be itself converted to $\underline{O}H^- + \underline{O}_2^-$, or it may abstract an electron from the oxide lattice and be converted to $\underline{O}_2^{2-} + \underline{O}^-$. The prospect of developing this type of OCM catalysts is discussed.

KEY WORDS: methane oxidative coupling; Th–La–O_x/$BaCO_3$; non-reducible rare-earth-oxide-based catalysts; surface oxygen species; $\underline{O}_3^{2-}$; $\underline{O}_2^-$; $\underline{O}_2^{2-}$; *in situ* Raman spectroscopy

1. Introduction

Certain supported or composite metal-oxides catalysts can catalyze the oxidative coupling of methane (OCM) to ethane and ethylene as well as to minor amounts of other C_{2+} hydrocarbons from CH_4–O_2 fed alternatively (redox cyclic-feed operation for OCM catalysts containing multivalent cations [1]), or simultaneously (co-feed operation [2] for OCM catalysts containing multivalent cations, or only valence-stable cations) through the catalyst bed. On account of the potentially practical significance in natural-gas resource utilization and the fundamental significance of methane activation, catalysis research on OCM has been the focus of worldwide attention for about a decade since the 8th ICC (Berlin, 1984). As shown by a more recent review [3], it has been established that OCM and side reactions are heterogeneous–homogeneous reactions initiated by H abstraction from gaseous phase CH_4 by active-oxygen species on the catalyst surface, liberating $\cdot CH_3$ radicals (along with co-produced H_2O), which couple mainly in the gas phase to form ethane as the primary product, and that ethylene are formed mainly by further reactions of C_2H_6 both heterogeneously and homogeneously, while by-products CO_x (i.e., CO_2 and CO) are formed by deep oxidation of any of the hydrocarbons on the catalyst surface and in the gas phase. It has been found that C_2 selectivity S (in %) decreases steadily with increasing CH_4 conversion, κ (in %); the maximum $\kappa + S$ that has been obtained so far is only about 100%. Obviously, as $\cdot CH_3$ and C_2H_4 in the reaction mixture increase in proportion relative to CH_4, their chances of further dehydrogenation and deep oxidation will also increase since the bond strength [4] of H–CH_3 ($\sim$440 kJ mol^{-1}) is only slightly smaller than that of H–CH_2 ($\sim$460 kJ mol^{-1}) or H–C_2H_3 ($\geqslant$452 kJ mol^{-1}). This is the main problem that has hampered the development of OCM to be a practical process for the direct production of ethylene from natural gas. However, with better understanding of the nature of active-oxygen species for OCM and the controlling factors for C_2 selectivity, the situation may be improved.

In the case of OCM catalysts containing multivalent cations, surface-lattice O^{2-} associated with cations in the oxidized state may be the active-oxygen species. Some OCM catalysts of this category have been found to show good activity and selectivity, with $\kappa + S$ around 100% [3,5]. However, OCM catalysts of this category generally require an alkali-ion promoter to modulate the oxidizing power of the multivalence metal oxide, and thus suffer from the disadvantage of gradual decline in activity and selectivity due to volatility loss of the alkali-ion promoter. OCM catalysts with valence-stable cations are practically inactive in CH_4 stream without O_2 [3,6], indicating that lattice O^{2-} associated with valence-stable cations is not an active-oxygen species.

The nature of active-oxygen species on non-reducible metal-oxide catalysts is still a matter of dispute [3]. Thus with alkali-doped alkaline-earth-oxide catalysts (e.g., the most thoroughly investigated Li^+/MgO), $\underline{O}^-$, $\underline{O}_2^{2-}$, and $\underline{O}_2^-$ have separately been considered to be the principal active-oxygen species for OCM [3,7,8]. However, $\underline{O}^-$ is known to be reactive toward C_2H_4 even at very low temperature [9], and the theoretical value of the energy barrier for H ab-

* Work supported by the National Priority Fundamental Research Project (No. G1999022400) of PR China.
** To whom correspondence should be addressed.

1011-372X/01/0500-0141$19.50/0

straction from H_3C–H by [$\underline{O}^-$–Li^+]/MgO has been shown by Borve and Pettersson [10] with the most refined model calculations to be only 25 kJ mol^{-1}, much smaller than the experimental value of 96 kJ mol^{-1} from kinetic measurements [11]. Some investigators [8] have suggested that $\underline{O}_2^-$ is less likely than $\underline{O}_2^{2-}$ to be a principal active-oxygen species for OCM since $\underline{O}_2^-$ is inactive around 723 K and readily liberates O_2 at higher temperature. However, $\underline{O}_2^-$ is most probably the precursor of $\underline{O}_2^{2-}$, which is known to be reactive towards CH_4 and C_2H_4 above 773 K, while the C_2 yield is known to increase with increasing temperature in the usual temperature range of OCM above 923 K; and Liu et al. [12] have argued that $\underline{O}_2^-$ may become active-oxygen species at OCM reaction temperature. Some direct evidence for $\underline{O}_2^-$ being reactive towards CH_4 at 973 K has been obtained by Wan et al. [13] with SrF_2/Nd_2O_3 and similar fluoride-containing rare-earth-oxide-based catalysts. For rare-earth-oxide-based catalysts, some investigators [14] have suggested that $\underline{O}_2^{2-}$ may be the principal active-oxygen species, and $\underline{O}_2^-$ formation may be sensitive to inhibition by surface carbonate. However, $\underline{O}_2^-$ formation on La_2O_3/CaO [15] has been found to be less sensitive to inhibition by CO_2 and surface carbonate than on undoped La_2O_3 [16].

Ex situ Raman spectroscopy was first used by Liu et al. [17] to study the $\underline{O}_2^-$, $\underline{O}_2^{2-}$, and surface carbonate species on a Cs^+/La_2O_3 catalyst in relation to the OCM catalytic activity, as well as the selectivity-promoting effect of CO_2 in O_2 stream used for reactivation of the catalyst. More recently, interesting results have been obtained from *in situ* Raman spectroscopic studies of active-oxygen species in OCM [18–23]. Thus Raman signals of $\underline{O}_2^{2-}$ on functioning La_2O_3, Na^+/La_2O_3, and Sr^{2+}/La_2O_3 at 973 K in flowing CH_4–O_2 feed as well as in O_2 stream have been reported by Mestl et al. [18]; and Raman signals (confirmed with $^{18}O_2$) of $\underline{O}_2^{2-}$ at 842 and 821 cm^{-1} (vw) from 0.5 mol% BaO/MgO in O_2 stream at 373 and 583 K (along with a very weak carbonate signal), shifting to very broad and weak band at 973 and 1073 K, have been observed by Lunsford et al. [19], who found that the $\underline{O}_2^{2-}$ adspecies reacted rapidly with CO_2 at OCM reaction temperature, especially in the presence of water vapor. With single-phase ThO_2–La_2O_3 of defective fluoride structure (DFS) [24] in CH_4–O_2 (4 : 1, v/v) co-feed stream, the weak Raman signal of $\underline{O}_2^-$ at 1140 cm^{-1} (w) (along with a very strong carbonate signal around 1060 cm^{-1} (vs)) has been observed by Liu et al. [20] at 1133 K with conspicuous increase in signal intensity with decreasing temperature; interestingly, the $\underline{O}_2^-$ Raman signal disappeared after switching the co-feed stream to pure O_2 stream at 1013 K and 0.1 MPa. Similar results have been reported by Cai et al. [21] with $(LaO)_2(O,CO_3)$–CaO/(Ba,Ca)CO_3 catalysts. With functioning Th–La–O_x/$BaCO_3$ catalyst (Th : La : Ba = 20 : 3 : 40, molar ratio) in CH_4–O_2 (4 : 1, v/v) stream at 1013 K and 2×10^4 h^{-1} GHSV, Raman signals at 1120 (w) and 1148 cm^{-1} (w) and at 812 (w) and 824 cm^{-1} (w) (assigned, respectively, to ν_{O-O} of two $\underline{O}_2^-$ adspecies and two $\underline{O}_2^{2-}$ adspecies in different microenvironments) have been observed by Zhang et al. [22,23], besides a very strong mono-dentate $C\underline{O}_3^{2-}$ Raman band centering around 1056 cm^{-1} (vs); after lowering the reaction temperature to 773 K, the two $\underline{O}_2^-$ signals were found to increase conspicuously in intensity (though still weak), while the two $\underline{O}_2^{2-}$ signals increased slightly in intensity, and a new band at 940 cm^{-1} (w) appeared, along with another weak $\underline{O}_2^{2-}$ band around 850 cm^{-1} (w).

These interesting observations have led us [23,25] to postulate that there might be an active and elusive precursor (of $\underline{O}_2^-$ and $\underline{O}_2^{2-}$), most probably a bent $\underline{O}_3^{2-}$ (with approximate C_{2v} symmetry and ν_1(A) at 940 cm^{-1}), which might be formed from reversible redox coupling of $\underline{O}_2$ (adsorbed at an anionic vacancy) with a neighboring O^{2-} in the surface lattice. However, more experimental and theoretical support for this assertion is required. For example, the possibility that the Raman signal at 940 cm^{-1} might be due to a lattice vibration or to peroxide and the structural adaptability of such a bent $\underline{O}_3^{2-}$ surface species must be carefully examined. Incidentally, the Th–La–O_x/$BaCO_3$ catalyst has been found in plug-flow microreactor evaluation to exhibit good C_2 yield and excellent thermal stability [26], but has failed in scale-up evaluation, probably due to hot spot over-heating and/or catalyst inactivation by CO_2 under oxygen-limiting conditions.

2. Experimental

2.1. Preparation of catalyst

A Th–La–O_x/$BaCO_3$ (Th : La : Ba = 10 : 0.2 : 10, molar ratio) catalyst was prepared from the aqueous nitrates by co-precipitation as carbonates and hydroxides, as reported previously [20]; the thoroughly washed precipitate was dried in air at 378 K, and ignited in air at 1123 K, then cooled down to room temperature and carefully pulverized and sieved to the desired mesh in a gloved box to avoid any physical contact with the hazardous thorium compounds. The sample was stored in closed vessel before use. In this preparation, lower proportions of Ba and La were used to lessen the extent of carbonate formation.

2.2. In situ Raman spectroscopic experiments

A horizontal quartz-tubular sample cell (with very uniform diameter of ~2.5 mm i.d.) heated with a tubular copper-block heater (with a small opening to accommodate the incident laser beams and scattered radiations and to facilitate visual observation of the hot spot) was used. The position of the sample cell (mounted together with the heater on a movable stand) could be forward-or-backward and upward-or-downward, as well as leftward-or-rightward, moved a few cm, and the incident laser beam was focused at the desired spot of the sample as indicated below. The quartz tubular sample cell also served as a plug-flow microreactor with 0.06 ml of 40–60 mesh catalyst sample filled to a length of

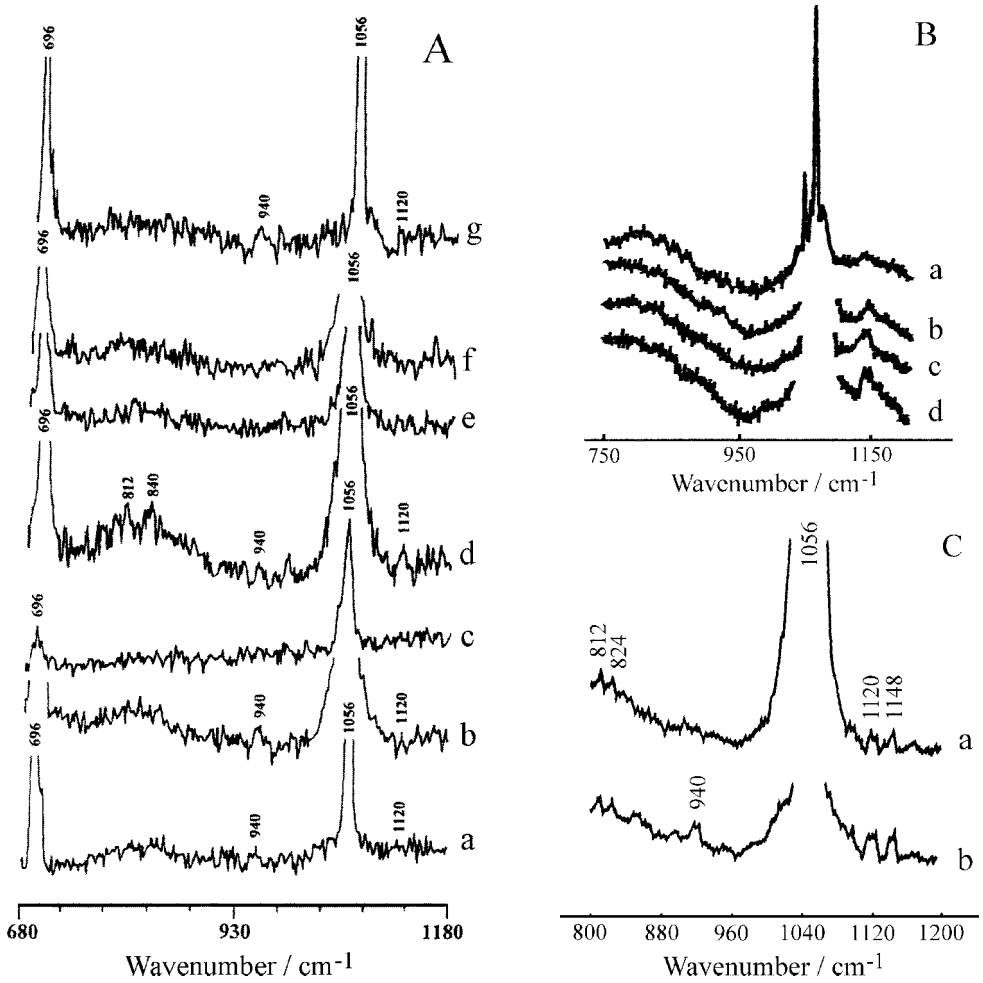

Figure 1. (A) Raman spectra of Th–La–O_x/$BaCO_3$ (Th : La : Ba = 10 : 0.2 : 10, molar ratio) catalyst taken at 0.1 MPa, 1×10^4 h^{-1} GHSV and under the following conditions: (a) Taken after exposing the fresh catalyst to O_2 stream at 648 K for 15 min, followed by lowering temperature to 383 K and switching to N_2 stream, and then lowering temperature to 298 K. (b) Taken with the sample after (a) and in CH_4–O_2 (4 : 1, v/v) stream at 973 K (at the hot spot), with the incident laser beam focusing at the spot of the sample about 1–2 mm up-stream from the hot spot of the functioning sample. (c) Taken at the same spot with the sample after (b) and exposing to CH_4 stream at 973 K for 5 min. (d) Taken at the same spot with the sample after (c) and exposing to CH_4–O_2 (4 : 1, v/v) stream at 773 K. (e) Taken at the same spot with the sample after (d) and exposing to CH_4 stream at 773 K for 5 min. (f) Taken with the sample after (e) and exposing to CH_4–O_2 (4 : 1, v/v) stream at 973 K (hot-spot temperature), but with the incident laser beam focusing on the spot of the sample about 1–2 mm down-stream from the hot spot of the functioning sample. (g) Taken at the same spot as in (f) with the sample after (f) and cooling to 648 K and then switching to O_2 stream, followed by cooling to 383 K and then switching to N_2 stream, and finally cooling to 298 K. (B) *In situ* Raman spectra of functioning ThO_2–La_2O_3 (Th : La = 7 : 3, molar ratio; DFS, single-phase) in CH_4–O_2 (4 : 1, v/v) stream at 0.1 MPa and (a) 1133, (b) 1073, (c) 1013 and (d) 953 K (reproduced from [20]). (C) *In situ* Raman spectra of functioning Th–La–O_x/$BaCO_3$ (Th : La : Ba = 20 : 3 : 40, molar ratio) in CH_4–O_2 (4 : 1, v/v) stream at 2.0×10^4 GHSV, and (a) 1013 and (b) 773 K (reproduced from [22,23]).

about 1.2 cm and placed between two quartz-wool plugs, and the preheating zone was filled with 40–60 mesh quartz chips. The temperature of the catalyst sample was registered with a tiny NiCr–NiAl thermocouple (in thin, stainless-steel sheath ca. 1.0 mm o.d.) placed right at the hot spot of the sample during the OCM reaction. *In situ* Raman spectra of the sample in different gaseous streams were taken by using a Spex Ramalog 6 laser Raman spectrometer, with the 514.5 nm line from a Coherent-Innova model 200 argon ion laser used as the excitation source. Slit width settings correspond to a resolution of 4 cm^{-1}. The laser beam (30 mW) was focused on the desired spot of the stationary sample (except that the tubular reactor was manually rotated at intervals) under various treatments as indicated in the legend of figure 1(A). Since the temperature of the sample appeared to be very uneven along the feed-gas stream around the hot spot during the OCM reactions, the oscillation of the sample tube was not carried out in this supplementary experiment.

3. Results and discussion

3.1. In situ Raman spectroscopic studies

Figure 1(A, curve (a)) shows that, from the ignited sample after exposure to O_2 stream at 648–383 K and cooling in N_2 stream to 298 K, weak but distinct Raman signal at 940 cm^{-1} (w) and weaker Raman signal around 1120 cm^{-1} (w) due to $\underline{O}_2^-$ were observed, along with a weak and very

broad band around 820–840 cm^{-1} probably due to $\underline{O}_2^{2-}$, besides two strong bands at 1056 and 696 cm^{-1} assigned to $\nu_{2(}A_1)$ and $\rho_{OCO}(B_2)$, of mono-dentate carbonate, $\underline{O}CO_2^{2-}$ [27], which were formed (in the preparation of sample) during the ignition in air usually containing 1 mol% CO_2. The features of *in situ* Raman spectra shown in curves (b) and (d) of figure 1 (A) taken with the functioning Th–La–O_x/$BaCO_3$ (Th : La : Ba = 10 : 0.2 : 10, molar ratio) catalyst with the incident laser beam focused at the same spot slightly up-stream of the sample (thus at temperature slightly below the hot-spot temperature 973 or 773 K for figure 1 (A(b)) or (A(d)), respectively) may be compared with that taken with functioning Th–La–O_x/$BaCO_3$ (Th : La : Ba = 20 : 3 : 40, molar ratio) catalyst at 1013 and 773 K (in slightly larger and vertically oscillating sample tube) shown in figure 1 (C(a)) and (C(b)) (in the insertion reproduced from [23]). It can be seen that the general features of figure 1 (A(d)) and (C(b)) appeared to be quite similar, in spite of the much lower level of doping with La^{3+} and slightly lower temperature (probably 20°–30° lower than 773 K) in the former case; and that in figure 1(A(b)) with the Raman spectrum taken at the same spot of the sample as in figure 1(A(d)) (and thus at temperature at least 30° lower than the hot-spot temperature 973 K), the 940 cm^{-1} signal was stronger, while the $\underline{O}_2^{2-}$ and $\underline{O}_2^-$ Raman signals both weaker than that shown in figure 1(A(d)) taken at temperature slightly lower than the hot-spot temperature of 773 K. In figure 1(C(a)) with the Raman spectrum taken at 1013 K, the Raman signal at 940 cm^{-1} could hardly be seen; thus it appeared to be an elusive species, existing only at temperature below 1013 K.

From the weaker Raman signal at 940 cm^{-1} (w) compared with that of $\underline{O}_2^{2-}$ and $\underline{O}_2^-$ shown in figure 1(A(d)) taken at ~773 K, and the stronger Raman signal at 940 cm^{-1} compared with that of $\underline{O}_2^{2-}$ and $\underline{O}_2^-$ shown in figure 1(A(b)) taken at ~973 K, as well as from the disappearance of this signal after short exposure of the sample to CH_4 stream at 973 or 773 K, as shown in figure 1 (A(c)) and (A(e)), the possibility of this 940 cm^{-1} signal being due to lattice vibration may be ruled out; it also appears very unlikely that this signal is due to a species of $\underline{O}_2^{2-}$. On the other hand, these results are in line with the assertion [23] that the 940 cm^{-1} signal might be due to an active precursor of $\underline{O}_2^{2-}$ and $\underline{O}_2^-$, most probably $\underline{O}_3^{2-}$ formed (with a gain in electron delocalization energy) by reversible redox coupling of $\underline{O}_2$ at an anionic vacancy with a neighboring O^{2-} in the surface lattice with adequate inter-nuclear distance between neighboring anions. This active precursor $\underline{O}_3^{2-}$ might react like a resonance hybrid [$\underline{O}_3^{2-} \leftrightarrow \underline{O}_2^- + \underline{O}^-$] in abstracting an electron from the oxide lattice and be itself converted to $\underline{O}_2^{2-} + \underline{O}^-$ since the electron affinity of $\underline{O}_2^-$ is greater than that of $\underline{O}^-$; or it might reversibly dissociate into $\underline{O}_2^- + \underline{O}^-$; or it might be active at the OCM reaction temperature in H abstraction from CH_4 and be itself converted to $\underline{O}_2^-$ plus $\underline{O}H^-$ since H abstraction by $\underline{O}^-$ is much stronger than by $\underline{O}_2^-$.

Since the surface site for the formation of this postulated active precursor $\underline{O}_3^{2-}$ conceivably overlaps with that of its down-stream species $\underline{O}_2^{2-}$ and $\underline{O}_2^-$, and since this active precursor appears to be thermally less stable than $\underline{O}_2^{2-}$ and, in H abstraction from CH_4, slightly less active than $\underline{O}_2^{2-}$, but more active than $\underline{O}_2^-$, the relative intensities of the observed Raman signals of these oxygen adspecies shown in figure 1 (A(d)) and (A(b)) may be interpreted as follows. In CH_4–O_2 (4 : 1, v/v) co-feed stream at the lower temperature slightly below 773 K, $\underline{O}_2^{2-}$ would not react very fast with CH_4, and $\underline{O}_2^-$ would be inactive at this low temperature in H abstraction from CH_4, so most of the anionic vacancies would be occupied at the steady state by these down-stream adspecies, $\underline{O}_2^{2-}$ and $\underline{O}_2^-$, and a relatively smaller number of anionic vacancies would be left for the adsorption of O_2 and the formation of $\underline{O}_3^{2-}$, resulting in weaker Raman signal of $\underline{O}_3^{2-}$ at 940 cm^{-1} (w) compared with that at 840–812 (w–m) and 1120 cm^{-1} (w–m) due to $\underline{O}_2^{2-}$ and $\underline{O}_2^-$, respectively, as shown in figure 1(A(d)). On the other hand, in the same co-feed stream at higher temperature (slightly below 973 K), most of the $\underline{O}_2^{2-}$ adspecies would be scavenged by the fast reaction with CH_4, and the $\underline{O}_2^-$ adspecies would also react with CH_4 to some extent, besides some extent of further reduction to $\underline{O}_2^{2-}$ by the oxide lattice, and some extent of thermal decomposition (slightly aided by the 30 mW laser-beam irradiation) with liberation of O_2; thus there would be more anionic vacancies at this higher temperature for the adsorption of O_2 and formation of $\underline{O}_3^{2-}$, as shown in figure 1(A(b)) by the stronger Raman signal at 940 cm^{-1} (w–m).

From figure 1(A(f)), it can be seen that under the OCM reaction conditions and at the spot of the catalyst sample about 1–2 mm down-stream from the hot spot at 973 K, there was no distinct *in situ* Raman signal for any of the oxygen adspecies mentioned above, indicating that O_2 appeared to be almost exhausted at a short distance down-stream from the hot spot. That means most of the catalyst sample down-stream from the hot spot was exposed to the reaction mixture rich in unconverted CH_4 and the C_{2+} products, as well as CO_x and H_2O(g), but almost exhausted in O_2. Note that over such highly active Th–La–O_x/$BaCO_3$-based catalysts under similar OCM reaction conditions, 94–98% conversion of O_2 in the CH_4–O_2 (4 : 1, v/v) co-feed at high GHSV has been observed from GC analysis of the microreactor effluents [26].

As shown in figure 1(A(g)), after switching the above sample to O_2 stream at 648–383 K and cooling to 298 K in N_2 stream, the Raman signal at 940 cm^{-1} (w–m) and that around 1120 cm^{-1} (w) could still be observed (along with the strong carbonate signal). Note that these two signals shown in figure 1(A(g)) were both of higher intensity than the corresponding signals shown in figure 1(A(a)) since in (a) exposure of the sample to O_2 stream at 648–383 K was started with a fresh sample ignited and cooled in air, while in (g) exposure of the sample to O_2 stream at 648–383 K was started after (f) in which almost all the active-oxygen adspecies at this part of the sample (down-stream past the hot

spot) could be well scavenged by the OCM reaction mixture rich in CH_4, C_{2+}, H_2O(g), and CO_x, but almost exhausted in O_2.

Incidentally, with the Th–La–O_x/$BaCO_3$-based catalysts on prolonged exposure of the catalyst sample in O_2 stream around or above 973 K, neither the 940 cm^{-1} Raman signal, nor the Raman signal of $\underline{O}_2^-$ around 1120–1150 cm^{-1}, could be observed. This is reminiscent of the disappearance of the Raman signal of $\underline{O}_2^-$ from either the La–Ba–Ca–O_x/$BaCO_3$ catalyst at 973 K [21], or the single-phase ThO_2–La_2O_3 catalyst at 1013 K [20] on prolonged exposure to O_2 stream, whereas with either of the last two catalysts in CH_4–O_2 co-feed stream at the corresponding temperature, distinct Raman signal of $\underline{O}_2^-$ has been observed even in the presence of very strong carbonate signals.

The disappearance of the Raman signal of $\underline{O}_2^-$ (in contrast to the presence of the $\underline{O}_2^{2-}$ signal) when a non-reducible metal-oxide catalyst for OCM is exposed to O_2 stream around 973 K is most probably explained as follows. The adspecies $\underline{O}_2^{2-}$ is formed via interaction of $\underline{O}_2$ with the oxide lattice in two steps with the formation of $\underline{O}_2^-$ as a precursor or intermediate, which is known to be thermally less stable than $\underline{O}_2^{2-}$ (though O_2^{2-} would be unstable as a free anion [28]). Though the formation of $\underline{O}_2^-$ is most probably faster than its further conversion to $\underline{O}_2^{2-}$, and an initial transient concentration of $\underline{O}_2^-$ might be built up, but it would soon decline, due to the gradual conversion of $\underline{O}_2^-$ to the thermally more stable $\underline{O}_2^{2-}$. At the steady state, most of the available anionic vacancies would be occupied by $\underline{O}_2^{2-}$, and the surface concentration of $\underline{O}_2^-$ might fall below the detection limit of the Raman spectrometer if the temperature is sufficiently high. However, in CH_4–O_2 co-feed stream at 973 K or higher OCM temperature, $\underline{O}_2^{2-}$ might react with CH_4 almost as fast as its formation from $\underline{O}_2^-$, thus most of the $\underline{O}_2^{2-}$ would be scavenged, leaving more anionic vacancies for the fast adsorption of O_2 and the formation of $\underline{O}_2^-$, which at sufficiently high OCM temperature (973 K or higher) may have a chance to react with CH_4 before its further conversion to $\underline{O}_2^{2-}$. By similar reasoning, the absence of the 940 cm^{-1} signal from the Th–La–O_x/$BaCO_3$ catalyst in O_2 stream around 973 K may be taken as an indication that this signal is due to an OCM-active (though apparently not as active as $\underline{O}_2^{2-}$) but thermally less stable precursor of $\underline{O}_2^-$ and $\underline{O}_2^{2-}$, and that the surface site for this precursor species overlaps with that for $\underline{O}_2^-$ and $\underline{O}_2^{2-}$. This again is in line with the suggestion that this active precursor is most probably $\underline{O}_3^{2-}$ formed via reversible redox coupling of $\underline{O}_2$ with a nearest O^{2-} in the surface lattice.

Conceivably, the higher thermal stability of $\underline{O}_2^{2-}$ is mainly due to the larger Madelung stabilization energy for the doubly charged $\underline{O}_2^{2-}$ compared with that for the singly charged $\underline{O}_2^-$ at the same anionic site of the surface lattice. Similarly, $\underline{O}_3^{2-}$ may be thermally more stable than an ozonide anion, $\underline{O}_3^-$, mainly due to the larger Madelung stabilization energy for $\underline{O}_3^{2-}$ compared with that for $\underline{O}_3^-$ at the same surface site.

It is desirable to examine the possibility of detecting the changes in the concentrations of $\underline{O}_3^{2-}$ and/or $\underline{O}_2^-$ as the transient precursors, and of $\underline{O}_2^{2-}$ as the thermally more stable adspecies, with time of exposure of a thoroughly degassed Th–La–O_x/$BaCO_3$ or a similar catalyst to O_2 stream around 973 K. The use of a fast spectrometer, e.g., a microfocus Raman spectrometer or a fast FT-IR spectrometer, will be tried.

It is also desirable to carry out isotopic tracing experiments with $^{18}O_2$ to confirm the assignment of the 940 cm^{-1} signal to ν_1(A) of $\underline{O}_3^{2-}$ from the characteristic frequency red-shifts, and to study the mechanism of isotopic exchange on the Th–La–O_x/$BaCO_3$-based catalysts. The reversible redox coupling of $^{18}\underline{O}_2$ with lattice O^{2-} to form $^{18}\underline{O}^{18}O^{16}\underline{O}$ followed by decoupling on this type of catalysts may lead to very fast isotopic exchange, liberating $^{18}O^{16}O$ as a primary product, as pointed out previously [23]. Note that fast isotopic exchange of $^{18}O_2$ with Ca^{2+}/ThO_2, or La_2O_3, or Sr^{2+}/La_2O_3, starting at about 773, 723 and 650 K, respectively, has been observed by Kalenik and Wolf [6], but no isotopic exchange at all with undoped ThO_2.

3.2. Structural adaptability for the formation of bent $\underline{O}_3^{2-}$

The frequency of the postulated $\underline{O}_3^{2-}$ species was estimated to be around 900–950 cm^{-1} from the known O–O stretching frequencies of O_2 (1580.4 cm^{-1} [27]), $\underline{O}_2^-$ ($\sim$1122 cm^{-1} for $Ba(O_2)_2$ [26]), $\underline{O}_2^{2-}$ ($\sim$840 cm^{-1} for BaO_2 [26]), and the known stretching frequencies ν_1(A) and structural parameters [29,30] of O_3 (ν_1 = 1134.9 cm^{-1} [27]; O1–O2 = 0.1278 nm, O1–O3 = 0.218 nm, bond angle = 116.7° [29]), and $\underline{O}_3^-$ (ν_1 = 1016 cm^{-1} [27,29]; O1–O2 = 0.135 nm, O1–O3 = 0.226 nm, bond angle = 113.5° [30]). Thus from O_3 to $\underline{O}_3^-$, a frequency red-shift of about 119 cm^{-1} has been observed from Raman spectroscopy. This is much smaller than the frequency red-shift of about 460 cm^{-1} from O_2 to $\underline{O}_2^-$, as expected. Nevertheless, this is in accord with the observed structural parameters and indicates that there are a small increase in bond length and decrease in bond order from O_3 to $\underline{O}_3^-$. From $\underline{O}_2^-$ to $\underline{O}_2^{2-}$, there is a considerably smaller frequency red-shift than from O_2 to $\underline{O}_2^-$ (ca. 280 cm^{-1} vs. ca. 460 cm^{-1}). It may be expected that from $\underline{O}_3^-$ to the postulated $\underline{O}_3^{2-}$, there would also be a frequency red-shift considerably smaller than that from O_3 to $\underline{O}_3^-$, though there would still be some partial bonding between the two terminal oxygens, O1 and O3.

The ν_1(A) of O_3 and $\underline{O}_3^{2-}$ might be compared with the stretching frequencies of the corresponding isoelectronic bidentate carboxylate ligands, e.g., $HCOO^-$ ($\nu_{OCO} \approx$ 1366 cm^{-1} [27], 1355 cm^{-1} [30]) or CH_3COO^- ($\nu_{OCO} \approx$ 1414 cm^{-1} [27], bond angle $\sim$ 121°, inter-nuclear distance between the two terminal oxygens $\sim$0.218 nm [30]), and a dioxymethylene bidentate ligand, μ-$H_2C\underline{O}_2^{2-}$ ($\nu_{OCO} \approx$ 1160 and 1130 cm^{-1} [31], ca. 200 cm^{-1} lower than that of $HCOO^-$). Incidentally, μ-$H_2C\underline{O}_2^{2-}$ has been proposed to be a surface reaction intermediate in the hydrogenation

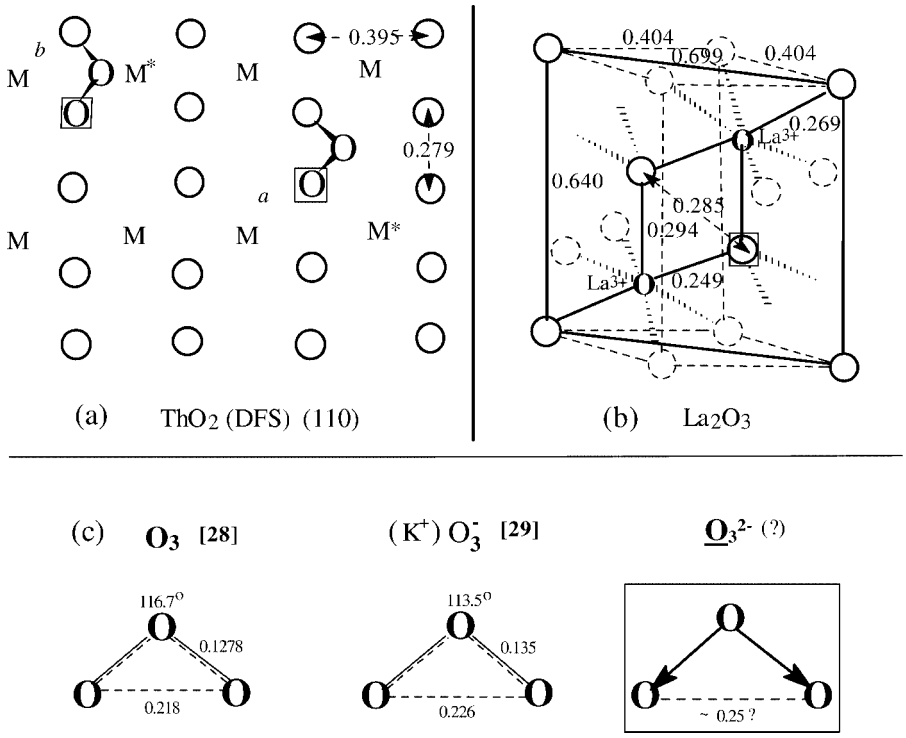

Figure 2. (a) (110) surface of ThO_2 (DFS by doping with La_2O_3 or BaO, SrO, CaO); M, M*, O, and square-bracketed O denote, respectively, Th(IV), La(III) or M(II), lattice oxide ion, and anionic vacancy. Formation of postulated bent $\underline{O}_3^{2-}$ from $\underline{O}_2$ adspecies (at an anionic vacancy) and a lattice O^{2-} are shown at two types of sites, *a* and *b*. (b) Unit-cell of hexagonal La_2O_3 (doped) with each La(III) ligated by 7 O^{2-} in mono-capped octahedral configuration. Solid lines and circles denote the non-polar (110) surface lattice. (c) Bent structure of O_3 and $\underline{O}_3^-$. Unit of length: nm.

of CO to methanol over Cu/ZnO-based catalyst [23,31]; μ-$H_2C\underline{O}_2^{2-}$ might also be formed in the adsorption of H_2CO on $ZnAl_2O_4$ [31], conceivably via coupling of H_2CO with a lattice O^{2-} (analogous to the redox coupling of $\underline{O}_2$ with O^{2-}).

From the above considerations, the frequency red-shift for $\underline{O}_3^-$ to $\underline{O}_3^{2-}$ may be only about 50–70% of that for O_3 to $\underline{O}_3^-$; i.e., ν_1 of $\underline{O}_3^{2-}$ may be estimated to be about 930–960 cm^{-1}; and the inter-nuclear distance about 0.25–0.26 nm, assuming that the bond angle may be about 116°–120°. This might be stretched to about 0.27–0.28 nm at the surface anionic site, from the consideration of surface Madelung stabilization energy (especially with multiply charged cations). The two electronic units of negative charge on $\underline{O}_3^{2-}$ would be more or less concentrated at the two terminal oxygens. Thus in the case of the doped ThO_2 (DFS) with the closest inter-anionic distance of about 0.279 nm in the non-polar (110) surface lattice, formation of $\underline{O}_3^{2-}$ via reversible redox coupling of $\underline{O}_2$ with a neighboring O^{2-} is highly probable, as shown in figure 2(a) in two different microenvironments, *a* and *b*. In the case of doped La_2O_3 shown in figure 2(b), the closest inter-nuclear distance between two neighboring anions in the non-polar (110) surface lattice is 0.285 nm, slightly larger than the sum of V.d.W. radii of the two terminal O; this would be marginal for the formation of $\underline{O}_3^{2-}$, so here such an active-oxygen species (if it could be formed transiently at all) might be too elusive to show any observable Raman signal. For Li^+/MgO and Na^+/CaO, both with rock salt structure for the host phase, formation of $\underline{O}_3^{2-}$ is improbable because of too large inter-nuclear distances, respectively, 0.297 and 0.340 nm, for two neighboring anions in the non-polar (100) surface lattice.

It is of fundamental interest to make refined quantum-chemical calculations with an appropriate cluster model for the energy of formation and the vibration frequencies of $\underline{O}_3^{2-}$ at the defective ThO_2 surface lattice shown in figure 2(a), as well as the energy barrier for the H abstraction from H–CH_3 by $\underline{O}_3^{2-}$.

3.3. Rational design of non-reducible rare-earth-oxide-based OCM catalysts

With the Th–La–O_x/$BaCO_3$-based OCM catalysts, the formation of $\underline{O}_3^{2-}$ from $\underline{O}_2$ via redox coupling with a neighboring O^{2-} is not accompanied with the formation of the undesirable O^- species in the surface lattice, in contrast with the formation of $\underline{O}_2^-$ from $\underline{O}_2$ via redox reaction with O^{2-} in the surface lattice with co-production of O^-.

The $\underline{O}_3^{2-}$ species may react neatly with CH_4 to produce a $\cdot CH_3$, and $\underline{O}_3^{2-}$ converted to $\underline{O}H^-$ plus $\underline{O}_2^-$, which is harmless to the $\cdot CH_3$ just formed, if collision occurs, since $\underline{O}_2^-$ may not be able to abstract an H from $\cdot CH_3$ because of the large difference in bond strengths [4] of H–$\underline{O}\underline{O}$ (ca. 364.8 kJ mol^{-1} for D^0 of H–OOH) vs. H–CH_2 (D^0 460 kJ mol^{-1}). At high enough OCM temperature $\underline{O}_2^-$ may be able to abstract an H from another CH_4 molecule (439.7 kJ mol^{-1} for D^0 H–CH_3) to produce one more $\cdot CH_3$. The two $\cdot CH_3$ radicals may have a high probability to cou-

ple and form C_2H_6. Thus in a series of comparative assays with stationary-bed microreactor, the Th–La–O_x/$BaCO_3$-based OCM catalysts have consistently been found by Liu et al. [26] to give 2–3% (absolute) higher C_{2+} yield than the La_2O_3/$BaCO_3$-based catalysts, which have been found to form $\underline{O}_2^-$, but no $\underline{O}_3^{2-}$ species, under OCM reaction conditions.

For further improvement of the non-reducible rare-earth-oxide-based catalysts, the active sites of the catalyst should be highly dispersed and methane conversion should be adequate, but not be too high, in order to obtain high C_2 selectivity at the industrially acceptable level of C_2 yield and to decrease the extent of the highly exothermic CO_2 formation so as to avoid excessive hot-spot overheating. A catalyst with DFS host phase and adequate internuclear distance between an anionic vacancy and its nearest anionic neighbor for the formation of the active precursor, $\underline{O}_3^{2-}$, and well-dispersed active sites would be desirable. But the use of hazardous thorium compound is undesirable. Probably, certain valence-stable M_2O_3-type lanthanide-oxide-based solid solution with cubic, defective fluorite structure may be used as the active phase. This must be well dispersed in a thermally stable carrier (e.g., $BaCO_3$), which may also serve as effective quencher of free-radical reactions in the gaseous phase [26]. This type of catalysts would not be robust enough for use in a fluidized-bed reactor. So a certain type of stationary-bed reactor must be designed, that would have the advantage of avoiding attrition loss of the catalyst. But then heat dissipation would become a formidable engineering problem.

4. Concluding remarks

It is now beyond doubt that on non-reducible rare-earth-oxide-based OCM catalysts, $\underline{O}_2^-$ may be observed by its Raman signal in the presence of a large amount of surface carbonate, and that this adspecies is most probably an active-oxygen species under OCM reaction conditions. The supplementary *in situ* laser Raman spectroscopic study of active-oxygen species on Th–La–O_x/$BaCO_3$ OCM catalyst and structural adaptability considerations have provided further support for the suggestion [23,25] that there might be an active and elusive precursor of $\underline{O}_2^-$ and $\underline{O}_2^{2-}$, most probably $\underline{O}_3^{2-}$ formed by reversible redox coupling of $\underline{O}_2$ with a neighboring O^{2-}. However, further studies of the transient adspecies with fast *in situ* Raman and FT-IR spectroscopic methods and of the mechanism of $^{18}O_2$ exchange with this type of non-reducible rare-earth-oxide-based catalysts, as well as refined quantum-chemical calculations of $\underline{O}_3^{2-}$ formation, vibration frequencies, and H-abstraction reactivity using appropriate surface-cluster models, are highly desirable. Such fundamental studies will be very helpful in rational design of this type of OCM catalysts.

References

[1] G.E. Keller and M.M. Bhasin, J. Catal. 73 (1982) 9.
[2] W. Hinsen, W. Bytyn and M. Baerns, in: *Proc. 8th Int. Congr. on Catalysis*, Vol. 3 (1984) p. 581.
[3] J.H. Lunsford, Angew. Chem. Int. Ed. Engl. 34 (1995) 970.
[4] *CRC Handbook of Chemistry and Physics*, 66th Ed. (CRC Press, Boca Raton, 1985).
[5] Z.C. Jiang, C.J. Yu, X.P. Fung, S.B. Li and H.L. Wang, J. Phys. Chem. 97 (1993) 12870.
[6] Z. Kalenik and E.E. Wolf, Catal. Today 13 (1992) 255.
[7] K.D. Campbell, E. Morales and J.H. Lunsford, J. Am. Chem. Soc. 109 (1987) 7900.
[8] M. Hatano and K. Otsuka, J. Chem. Soc. Faraday Trans. 85 (1989) 199.
[9] M. Che and G.C. Bond, eds., *Adsorption on Oxide Surfaces*, Stud. Surf. Sci. Catal., Vol. 21 (Elsevier, Amsterdam, 1985) pp. 1, 11.
[10] K.J. Borve and L.G.M. Pettersson, J. Phys. Chem. 95 (1991) 3214.
[11] M. Xu, C. Shi, X. Yang, M.P. Rosynek and J.H. Lunsford, J. Phys. Chem. 96 (1992) 6395.
[12] Y.D. Liu, G.D. Lin, H.B. Zhang and K.R. Tsai, in: *Natural Gas Conversion II*, Stud. Surf. Sci. Catal., Vol. 81, eds. H.E. Curry-Hyde and R.F. Howe (Elsevier, Amsterdam, 1994) p. 131.
[13] H.L. Wan, X.P. Zhou, W.Z. Weng, R.Q. Long, Z.S. Chao, W.D. Zhang, M.S. Chen, J.Z. Luo and S.Q. Zhou, Catal. Today 51 (1999) 161.
[14] J.L. Dubois and C.J. Camron, Appl. Catal. 67 (1990) 49.
[15] T.L. Yang, L.B. Feng and S.K. Shen, J. Catal. 145 (1994) 384.
[16] C. Louis, T.L. Chang, M. Kermarec, T.L. Van, J.M. Taibouet and M. Che, Catal. Today 13 (1992) 283.
[17] Y.D. Liu, G.D. Lin, H.B. Zhang, J.X. Cai, H.L. Wan and K.R. Tsai, in: *Prepr. Fuel Chem. Div., ACS Nat. Mtg.*, San Francisco, 1992, Vol. 37(1), p. 356.
[18] G. Mestl, H. Knözinger and J.H. Lunsford, Ber. Burnsenges Phys. Chem. 97 (1993) 319.
[19] J.H. Lunsford, X. Yung, K. Haller, J. Laane, G. Mestl and H. Knözinger, J. Phys. Chem. 97 (1993) 13810.
[20] Y.D. Liu, H.B. Zhang, G.D. Lin, Y.Y. Liao and K.R. Tsai, J. Chem. Soc. Chem. Commun. (1994) 1871.
[21] J.X. Cai, A.M. Huang, Y.Y. Liao and H.L. Wan, in: *Proc. 4th Int. Conf. Raman Spectroscopy*, eds. N.T. Yu and X.Y. Li (Wiley, New York, 1994) p. 526.
[22] H.B. Zhang, Y.D. Liu, G.D. Lin, Y.Y. Liao and K.R. Tsai, Abstracts of Papers PHYS 0277, ACS Nat. Mtg., San Diego, 1994.
[23] K.R. Tsai, D.A. Chen, H.L. Wan, H.B. Zhang, G.D. Lin and P.X. Zhang, Catal. Today 51 (1999) 3.
[24] A.G. Anshits, E.N. Voskesenkaya and L.I. Kurteeva, Catal. Lett. 6 (1990) 49.
[25] K.R. Tsai, H.B. Zhang, G.D. Lin, H.L. Wan, Y.D. Liu, W.Z. Weng, J.X. Cai and Y.F. Shen, Abstracts of Papers CATL 028, ACS Nat. Mtg., Boston, 1998.
[26] Y.D. Liu, H.B. Zhang, G.D. Lin and K.R. Tsai, in: *Catalysis in C_1 Chemistry*, eds. K.R. Tsai, S.Y. Peng et al. (Chem. Ind. Press, Beijing, 1995) p. 46.
[27] K. Nakamoto, *Infrared and Raman Spectra of Inorganic and Coordination Compounds*, 4th Ed. (Wiley, New York, 1986) pp. 104, 112, 232, 255.
[28] A. Bielansky and J. Habor, Catal. Rev. Sci. Eng. 19 (1979) 1.
[29] N.N. Greenwood and A. Earnshaw, *Chemistry of the Elements* (Pergamon, Oxford, 1984) p. 707.
[30] T.C.W. Mak and G.D. Zhou, *Crystallography in Modern Chemistry* (Wiley, New York, 1992) p. 392.
[31] A. Vallet, C. Chauvin, J.C. Lavalley and P. Chaumette, J. Mol. Catal. 42 (1987) 205.